Supplementary Materials

Methyltransferase Inhibitors Restore SATB1 Protective Activity Against Cutaneous T Cell Lymphoma In Mice

Carly M. Harro*, Jairo Perez-Sanz*, Tara Lee Costich, Kyle K. Payne, Carmen M. Anadon, Ricardo A. Chaurio, Subir Biswas, Gunjan Mandal, Kristen E. Rigolizzo, Kimberly B. Sprenger, Jessica A. Mine, Louise C. Showe, Xiaoqing Yu, Kebin Liu, Paulo C. Rodriguez, Javier Pinilla-Ibarz, Lubomir Sokol, ‡Jose R. Conejo-Garcia

*Both authors contributed equally to this work.

‡Corresponding author

This PDF File includes:

Supplemental Materials and Methods

RNA-seq

Total RNA was collected from HuT78 cells at 72hrs using a Qiagen RNAesy Mini Kit and treated with RNAse-Free DNAse, Qiagen, Cat#79254 for removal of genomic DNA. Sequencing libraries were prepared by using NuGEN Universal RNA-Seq kit and run on NextSeq v2 300 cycles (75x2). Read depth was approximately ~35M reads per sample, and raw sequencing reads were trimmed and aligned to human genome assembly GRCh37 using STAR (32) (version 2.5.3a). Uniquely mapped reads were counted by htseq-count (33) (version 0.6.1) using Gencode v30 annotation. Differential expression analysis was performed using DESeq2 taking into account of RNA composition bias (34) and genes were ranked based on –log10(p-value)*(sign of log2(fold-change)). The ranked gene list was used to perform pre-ranked gene set enrichment analysis (GSEA version 4.0.2) (35) to assess enrichment of hallmarks, Reactome, and Gene Ontology (36) terms in MSigDB (36). The resulting normalized enrichment score (NES) and FDR controlled p-values were used to assess the transcriptome changes induced by F5446 and Chaetocin.

ChIP-seq

Samples were prepared in a similar method to the aforementioned ChIP section. Chromatin immunoprecipitation sequencing (ChIP-seq) was performed by the Molecular Genomics Core Facility at the Moffitt Cancer Center. Ten nanograms of immunoprecipitated DNA was fragmented to 300 base pairs using a Covaris M220 Focused-ultrasonicator (Covaris, Inc.,

Woburn, MA) and then used to generate sequencing libraries using the Kapa HyperPrep Kit (Roche Sequencing and Life Science, Wilmington, MA). The size and quality of the library was evaluated using the Agilent BioAnalyzer, and the library was quantitated with the Kapa Library Quantification Kit. Each enriched DNA library was then sequenced on an Illumina NextSeq 500 sequencer to generate 50 million 75-base paired-end reads (Illumina, Inc., San Diego, CA) (37). Sequencing adaptors and low-quality bases were trimmed off from the raw sequencing reads using cutadapt (38). Processed reads were aligned to human reference genome GRCh37 using Bowtie2 (37) and further filtered to remove discordant read pairs and reads with low alignment scores. Strand cross-correlation (SCC) analysis and calculation of NSC (normalized strand coefficient) and RSC (relative strand coefficient) values were performed using phantompeakqualtools. Narrow peaks were called by MACS2 (39) for histone marker H3K27ac with a minimal cutoff at narrow peak q-value (nq) <0.05. Broad peaks were called by MACAS2 for histone markers H3K27m3 and H2K9m3 with a minimal cutoff at nq<0.05 and broad peak q-value (bp) <0.05. The enriched reads and peaks were further annotated and analyzed using Chipseeker (40), deeptools (41), and ngsplot (42). Peak regions were lifted over to GRCh38 for primer design purpose using UCSC lift-over online tool (https://genome.ucsc.edu/cgi-bin/hgLiftOver).

REFERENCES

32. Dobin A, Davis CA, Schlesinger F, Drenkow J, Zaleski C, Jha S, et al. STAR: ultrafast universal RNA-seq aligner. *Bioinformatics (Oxford, England).* 2013;29(1):15-21.

33. Anders S, Pyl PT, and Huber W. HTSeq--a Python framework to work with high-throughput sequencing data. *Bioinformatics (Oxford, England).* 2015;31(2):166-9.

34. Love MI, Huber W, and Anders S. Moderated estimation of fold change and dispersion for RNA-seq data with DESeq2. *Genome biology.* 2014;15(12):550.

35. Subramanian A, Tamayo P, Mootha VK, Mukherjee S, Ebert BL, Gillette MA, et al. Gene set enrichment analysis: a knowledge-based approach for interpreting genome-wide expression profiles. *Proceedings of the National Academy of Sciences of the United States of America.* 2005;102(43):15545-50.

36. Ashburner M, Ball CA, Blake JA, Botstein D, Butler H, Cherry JM, et al. Gene ontology: tool for the unification of biology. The Gene Ontology Consortium. *Nature genetics.* 2000;25(1):25-9.

37. Langmead B, and Salzberg SL. Fast gapped-read alignment with Bowtie 2. *Nature Methods.* 2012;9(4):357-9.

38. Martin M. Cutadapt removes adapter sequences from high-throughput sequencing reads. *2011.* 2011;17(1):3.

39. Zhang Y, Liu T, Meyer CA, Eeckhoute J, Johnson DS, Bernstein BE, et al. Model-based analysis of ChIP-Seq (MACS). *Genome biology.* 2008;9(9):R137.

40. Yu G, Wang LG, and He QY. ChIPseeker: an R/Bioconductor package for ChIP peak annotation, comparison and visualization. *Bioinformatics (Oxford, England).* 2015;31(14):2382-3.

41. Ramírez F, Ryan DP, Grüning B, Bhardwaj V, Kilpert F, Richter AS, et al. deepTools2: a next generation web server for deep-sequencing data analysis. *Nucleic acids research.* 2016;44(W1):W160-5.

42. Shen L, Shao N, Liu X, and Nestler E. ngs.plot: Quick mining and visualization of next-generation sequencing data by integrating genomic databases. *BMC genomics.* 2014;15:284.

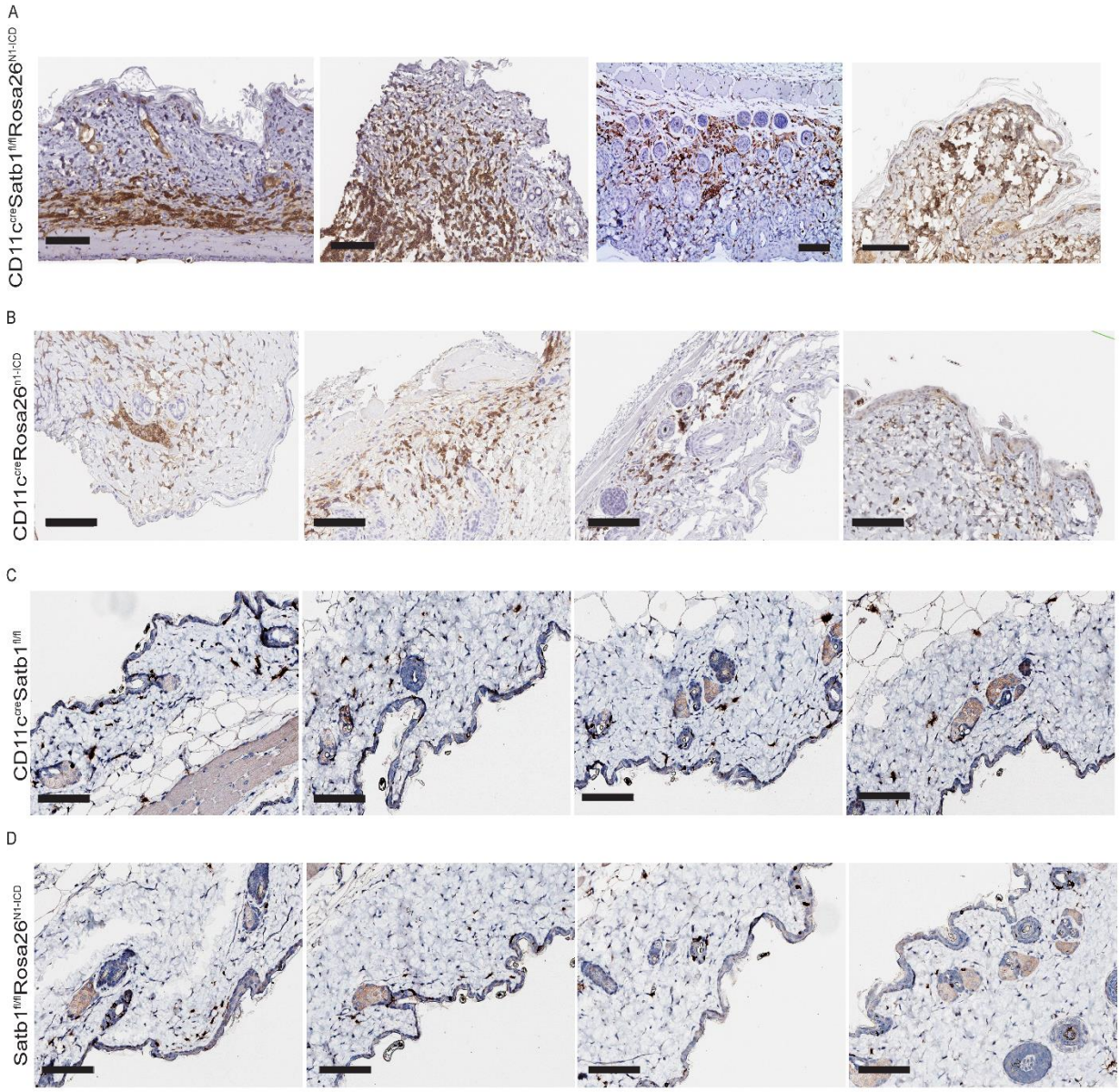

Supplemental Figure 1. Immunohistochemistry staining for CD3^{+} T-cell infiltration in mouse skin for CD11cCre model. Dermis and epidermis of mice show peripheral staining of CD3 in (**A**) *CD11c*$^{\mathrm{Cre}}$*Satb1*$^{\mathrm{flx/}flx}$*Rosa26*$^{N1\text{-}ICD}$ (n=4), (**B**) *CD11c*^{Cre}*Rosa26*$^{N1\text{-}ICD}$ (n=4), (**C**) *CD11c*$^{\mathrm{Cre}}$*Satb1*$^{\mathrm{flx/flx}}$ (n=4), and (**D**) *CD11c*$^{\mathrm{Cre}}$ negative (n=4) genotypes. Scale, 100um.

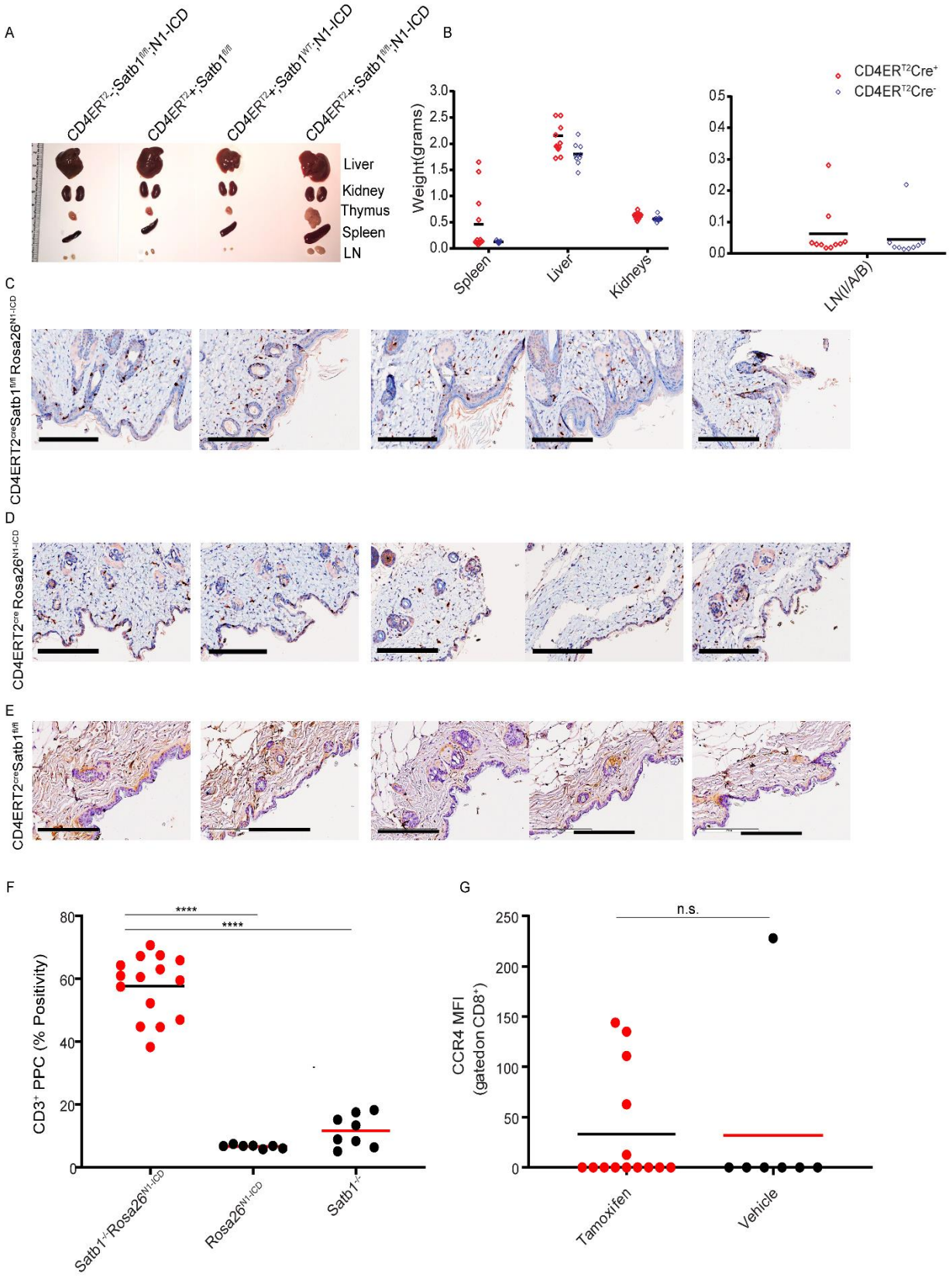
A
CD4ER^{T2}-;Satb1$^{fl/fl}$;N1-ICD
CD4ER^{T2}+;Satb1$^{fl/fl}$
CD4ER^{T2}+;Satb1^{WT};N1-ICD
CD4ER^{T2}+;Satb1$^{fl/fl}$;N1-ICD
Liver
Kidney
Thymus
Spleen
LN
B
Weight(grams)
Spleen
Liver
Kidneys
CD4ER^{T2}Cre^{+}
CD4ER^{T2}Cre^{-}
LN(I/A/B)
C
CD4ERT2^{cre}Satb1$^{fl/fl}$ Rosa26^{N1-ICD}
D
CD4ERT2^{cre}Rosa26^{N1-ICD}
E
CD4ERT2^{cre}Satb1$^{fl/fl}$
F
CD3^{+} PPC (% Positivity)
****
****
Satb1$^{+/-}$Rosa26^{N1-ICD}
Rosa26^{N1-ICD}
Satb1$^{+/-}$
G
CCR4 MFI (gatedon CD8^{+})
n.s.
Tamoxifen
Vehicle

Supplemental Figure 2. Organ weight and immunohistochemistry staining for CD3$^+$ T-cell infiltration in mouse skin for *CD4^{Cre}ER^{T2}* model. (**A**) Representative photo of liver, kidney, thymus, spleen and inguinal lymph nodes were from *CD4*^{Cre}*ER*^{T2}*Satb1*$^{flx/flx}$*Rosa26*$^{N1\text{-}ICD}$, *CD4*^{Cre}*ER*^{T2}*Rosa26*$^{N1\text{-}ICD}$, *CD4*^{Cre}*ER*^{T2}*Satb1*$^{flx/flx}$ and *CD4*^{Cre}*ER*^{T2} negative genotypes (2 replicates). (**B**) Organ weights of liver (n=10), kidney (n=10), spleen (n=10), and inguinal, axillary, and bilateral lymph nodes (n=10). Peripheral staining of CD3 in was shown in the dermis and epidermis of (**C**) *CD4Ert2*^{Cre}*Satb1*$^{flx/flx}$*Rosa26*$^{N1\text{-}ICD}$ (n=4), (**D**) *CD4Ert2*^{Cre}*Rosa26*$^{N1\text{-}ICD}$ (n=4), and (**E**) *CD4Ert2*^{Cre}*Satb1*$^{flx/flx}$ (n=4). Scale, 200um. (**F**) Quantitative Representation of Positive Pixel Count (PPC) of CD3+ staining of skin from (**C**) *CD4Ert2*^{Cre}*Satb1*$^{flx/flx}$*Rosa26*$^{N1\text{-}ICD}$ (n=15), (**D**) *CD4Ert2*^{Cre}*Rosa26*$^{N1\text{-}ICD}$ (n=7), and (**E**) *CD4Ert2*^{Cre}*Satb1*$^{flx/flx}$ (n=8). One-way ANOVA using multiple comparisons Tukey's test; ****$p \leq 0.0001$. (**G**) Median fluorescence intensity (MFI) of the expression of CCR4 in CD3$^+$CD8$^+$ T cells in the peripheral blood of *CD4*^{Cre}*ER*^{T2}*Satb1*$^{flx/flx}$*Rosa26*$^{N1\text{-}ICD}$ mice treated with tamoxifen (n=14) versus corn oil (n=7). Two-tailed Student's t-tests.

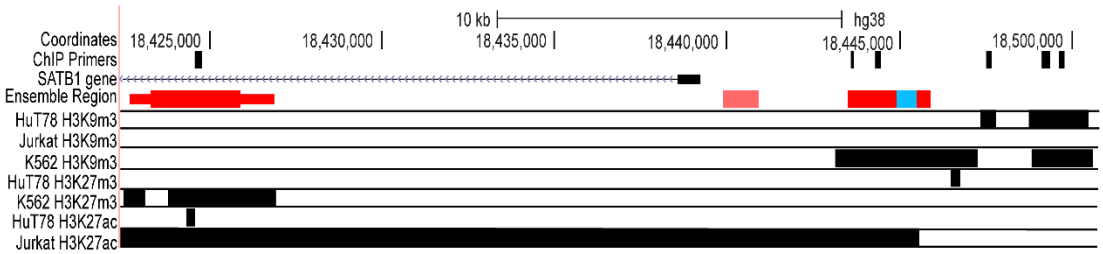

Supplemental Figure 3. Peaks adjacent to *SATB1* promoter in HuT78, Jurkat, K562 cell lines for ChIP pulled down for H3K27ac, H3K27me3, and H3K9me3 antibodies. Peak calling was generated using MACS2 with minimal cut off at nq<0.05 for narrow peaks and nq<0.05, bq<0.01 for broad peaks near the TSS of *SATB1* gene. Primers for ChIP-PCR analysis represented by their genomic coordinates on chromosome 3.

F5446.vs.DMSO

Chaetocin.vs.DMSO

Supplemental Figure 4. Categorized Pre-ranked GSEA on HuT78 cell line treated with F5446 and Chaetocin. Gene sets with FDR ≥0.05 were grouped into subcategories based on $CD4^+$ T cell function, interferon response, proliferation and cellular senescence, methyltransferase activity, histone modification, RNA processing, DNA replication, and nucleosome.

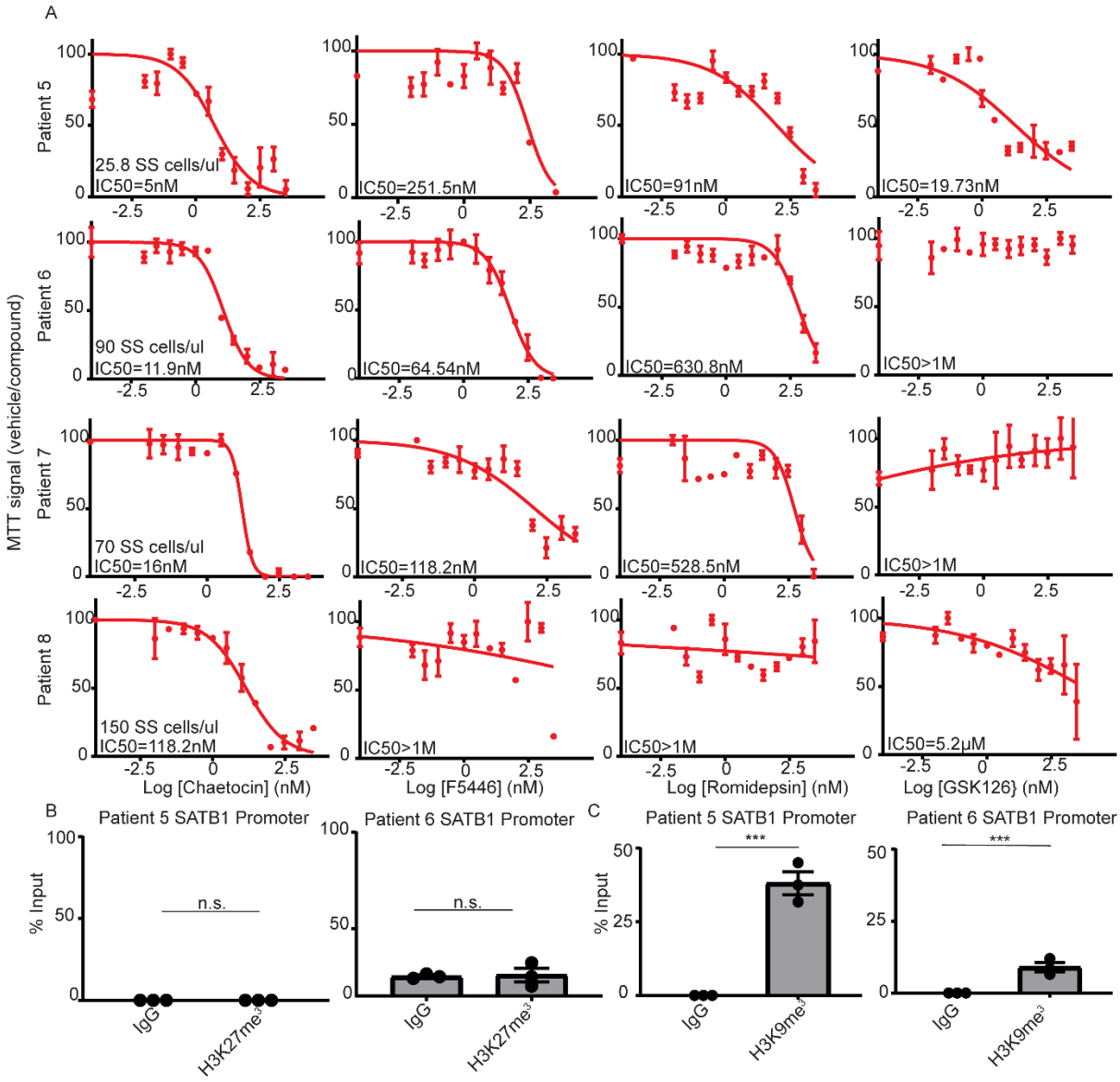

Supplemental Figure 5. H3K9me^3 repression of *SATB1* in CD4$^+$ T cells of Sézary patients. (**A**) CD4$^+$ only isolated T-cells from peripheral blood apheresis of Sézary patients (n=4) were cultured in R10 media with 100U/ml of human recombinant IL-2 and treated with increasing doses of SUV39H1/2 inhibitors Chaetocin and F5446 (72hrs) as well as GSK126 (48hrs) and romidepsin (72hrs) versus vehicle control (DMSO) prior to MTT analysis. IC_{50} values (nM) were calculated for each patient sample for the respective treatments. Representative of 2 independent experiments. (**B**) Chromatin Immunoprecipitation quantified by Real-Time Q-PCR with anti-H3K27me3

(clone#C36B11) or control IgGs pull downs from isolated $CD4^+$ T cells from peripheral blood of Sézary patients (n=2) calculated against 2.5% input values. Regions amplified at predicted occupied region (~4.8kb) SATB1 promoter (**C**) Similar to (**B**) except with anti-H3K9me3 (ab8898) at ~5.6kb region versus the control region (n=2). Representative of two independent experiments. Two-tailed Student's t-tests; ***$p \leq 0.001$

Supplemental Table 1. Peak calling for narrow and broad peaks from ChIP-seq analysis for HuT78, Jurkat, K562, and RAJI cell lines pulled down for H3K27ac, H3K27me3, and H3K9me3 antibodies. Peaks analysis with minimal cut off at nq<0.05 for narrow peaks and nq<0.05, bq<0.01 for broad peaks for cells lines HuT78, Jurkat, and K562 for all histone markers near the TSS of *SATB1* gene.

Supplemental Table 2. Categorized Pre-ranked GSEA using RNA-seq data for HuT78 treated with epigenetic inhibitors. Gene sets with FDR ≥0.05 were grouped into subcategories based on $CD4^+$ T cell function, interferon response, proliferation and cellular senescence, methyltransferase activity, histone modification, RNA processing, DNA replication, and nucleosome for all replicates and treatments of HuT78 cells at 72hrs.

Supplemental Table 3. Differential Gene (DE) expression and fold change for RNA-seq data for HuT78 treated with Chaetocin, F5446, and romidepsin. Differential Gene Expression analysis for all replicates and treatments of HuT78 cells at 72hrs.